

# Flexible Bond and Angle, FBA/ $\epsilon$ model of water

Raúl Fuentes-Azcatl\* and Marcia C. Barbosa\*

*Instituto de Física, Universidade Federal do Rio Grande do Sul, Caixa Postal 15051, CEP  
91501-970, Porto Alegre, RS, Brazil*

E-mail: razcatl@xanum.uam.mx; marcia.barbosa@ufrgs.br

## Abstract

We propose a new flexible force field for water. The model in addition to the Lennard-Jones and electrostatic parameters, includes the flexibility of the OH bonds and angles. The parameters are selected to give the experimental values of the density and dielectric constant of water at 1 bar at 240K and the dipole moment of minimum density. The FBA/ $\epsilon$  reproduces the experimental values of structural, thermodynamic and the phase behavior of water in a wide range of temperatures with better accuracy than atomistic and other flexible models. We expect that this new approach would be suitable for studying water solutions.

## Introduction

Water is ubiquitous in nature and strongly affects other materials when is in solution. This simple molecule, two hydrogen atoms linked to the oxygen by a covalent bond. In gas phase the HOH angle is  $104,474^\circ$  and the distance between oxygen and each hydrogen in  $0.095718\text{ nm}$ .<sup>1</sup> This angular structure is not fixed. In the liquid phase at  $298\text{ K}$  and  $1\text{ bar}$  it reaches the angle of 106 degrees.<sup>2</sup> Since the electrons in the covalent *HO* bond are strongly attracted to the oxygen, water is polarized with the region of the oxygen negative and the region of the hydrogen positive. Consequently the oxygen of one water attracts the hydrogen of the other water molecule forming the hydrogen bonding. Water due to the HOH angular structure can form up to four hydrogen bonds what leads to the tetrahedral structure which can aggregate in octamers. Then a small angular difference in the HOH covalent bonds can be relevant to the cluster structure of water.

In order to give a description of thermodynamic and dynamic properties of water, a number of non-polarizable models have been developed. The idea is to adjust the interaction potential between the molecules so the simulations reproduce the experimental value of a property such as the density at a certain temperature and pressure. This process has generated rigid models, manageable computationally, which give accurate values for a wide

range of thermodynamic and dynamic functions. However, since the potentials are fitted at a specific pressure and temperature, they are not able to cover different thermodynamic phases.

This rigid models are unable to capture the changes in the water polarization due to variations in temperature and pressure. This becomes particularly problematic when water is mixed with ionic or hydrophilic solutes. For instance, the rigid models do not reproduce the increase of the excess of specific heat when alcohol <sup>3</sup> is added to water and they are unable to explain the enhancement of the self-diffusion of water in the presence of certain electrolytes .<sup>4</sup> From the desire to produce an atomistic model which accounts for changes in the HOH water angle, without the computational costs of the ab initio simulations, a number of flexible models were introduced. Some of them were based in original non-polarizable models such as the SPC/E<sup>5</sup> and the TIP4P/2005<sup>6</sup> with the addition of more degrees of freedom. With this new approach, accurate water transport and other thermophysical properties were obtained,<sup>5-8,13</sup> however, these models fail in reproduce other thermodynamic and dynamic properties.<sup>5,13</sup> For instance, they do not give good estimates of the charge distribution.<sup>5,9-12</sup> Therefore, a good flexible model is still missing.

In this work we address this issue by following the same strategy adopted by Wu et al.<sup>5</sup> and Gonzalez and Abascal<sup>6</sup> by starting with a rigid non-polarizable model, the SPC/ $\epsilon$ <sup>14</sup> and introducing flexible bonds and angles. The idea is to combine the parametrization method employed for rigid model with the flexibility which adds additional degrees of freedom for the parametrization. We selected the rigid SPC/ $\epsilon$ <sup>14</sup> as an starting point due to its simplicity and because the rigid model already give some thermodynamic<sup>14</sup> and dynamic properties<sup>15</sup> close to the experimental results at room temperature and pressures.

The paper is organized as follows: Section 2 gives the force field of FBA/ $\epsilon$  model of water, followed by the details of the simulation and pursuit the parameters, Section 3 gives the properties of FBA/ $\epsilon$  compared with the non polarizable models and experimental values and in Section 4 the conclusions.

## The FBA/ $\epsilon$ force field

The Flexible Bond and Angle (FBA/ $\epsilon$ ) model is illustrated in the Figure 1. The molecule is represented by three sites. The oxygen attracts the negative charge while the hydrogens have the positive charge. The bonds and angles are not fixed but oscillate. The interaction potential exhibits the following contributions:

$$U(r) = U_{LJ}(r) + U_e + U_k(r) + U_\theta . \quad (1)$$

In the Eq. 1, the Lennard-Jones describes the intermolecular interactions between the massive particles, the oxygens, and the potential is given by

$$U_{LJ}(r) = 4\epsilon_{\alpha\beta} \left[ \left( \frac{\sigma_{\alpha\beta}}{r} \right)^{12} - \left( \frac{\sigma_{\alpha\beta}}{r} \right)^6 \right] \quad (2)$$

where  $r$  is the distance between the oxygens of two neighbor molecules  $\alpha$  and  $\beta$ ,  $\epsilon_{\alpha\beta}$  is the LJ energy scale and  $\sigma_{\alpha\beta}$  the repulsive diameter for an  $\alpha\beta$  pair. The cross interactions are obtained using the Lorentz-Berthelot mixing rules,

$$\sigma_{\alpha\beta} = \left( \frac{\sigma_{\alpha\alpha} + \sigma_{\beta\beta}}{2} \right); \quad \epsilon_{\alpha\beta} = (\epsilon_{\alpha\alpha}\epsilon_{\beta\beta})^{1/2} . \quad (3)$$

The coulomb forces between oxygen and hydrogen charges of the same or different molecules are represented by

$$U_e(r) = \frac{1}{4\pi\epsilon_0} \frac{q_\alpha q_\beta}{r} \quad (4)$$

where  $r$  is the distance between sites  $\alpha$  and  $\beta$ ,  $q_\alpha(\beta)$  is the electric charge of site  $\alpha(\beta)$  and  $\epsilon_0$  is the permittivity of vacuum.

The difference between the rigid SPC/ $\epsilon$  and the FBA/ $\epsilon$  model is the introduction in the

same molecule the intramolecular harmonic potentials in the bonds

$$U_k(r) = \frac{k_r}{2}(r - r_0)^2 \tag{5}$$

and in the angle.

$$U_\theta(\theta) = \frac{k_\theta}{2}(\theta - \theta_0)^2, \tag{6}$$

where  $r$  is the bond distance and  $\theta$  is the bond angle. The subscript 0 denotes their equilibrium values,  $k_r$  and  $k_\theta$  are the corresponding spring constants. The model has the following

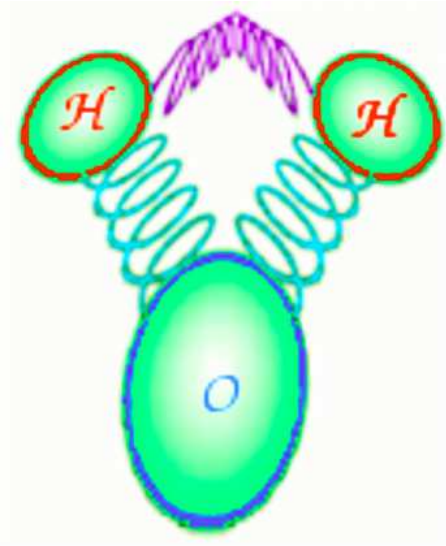


Figure 1: model of water including the harmonic potential in bonds and angle.

parameters:  $\epsilon_{\alpha\beta}$ ,  $\sigma_{\alpha\beta}$ ,  $q_\alpha$ ,  $q_\beta$ ,  $r_0$ ,  $\theta_0$ ,  $k_r$  and  $k_\theta$ . The parameterization procedure is the same employed in previous publication and goes as follows.<sup>16</sup>  $\epsilon_{\alpha\beta}$ ,  $\sigma_{\alpha\beta}$ ,  $q_\alpha$  and  $q_\beta$  were defined by requiring that the model reproduces: the density of liquid water, dielectric constant and dipole moment at 1 *bar* and 240K and the melting temperature at 1 *bar*. The idea behind is approach is to develop a flexible model which reproduces the bulk thermodynamic and dynamic properties of the equivalent rigid model for the pure system, but due to the flexibility is able to provide better results in mixtures or in confined geometries.

**Table 1: Parameters of the three-site water models considered in this work.**

model	$k_b$ kJ/ <i>mol</i> Å <sup>2</sup>	$r_{OH}$ Å	$k_a$ kJ/ <i>mol</i> rad <sup>2</sup>	$\Theta$ deg	$\varepsilon_{OO}$ kJ mol	$\sigma_{OO}$ Å	$q_O$ e	$q_H$ e
SPC/E <sup>14</sup>	-	1.000	-	109.45		3.1660	-0.8476	0.4238
SPC/ε <sup>14</sup>	-	1.000	-	109.45		3.1785	-0.8900	0.4450
FBA/ε	3000	1.027	383	114.70	0.792324	3.1776	-0.8450	0.4225
SPC/Fw <sup>5</sup>	4236.648	1.012	317.56	113.24	0.650299	3.165492	-0.8200	0.4100

## Simulation Details

We performed molecular dynamics simulations in the isothermal-isobaric ensemble, NPT, with isotropic fluctuations of volume, to compute the liquid properties at different temperatures and standard pressure, 1 *bar*. These simulations involved typically 500 molecules.

In order to compute the surface tension we used the constant volume and temperature ensemble, NVT, and 5832 molecules. We obtained the liquid-vapor interface by setting up a liquid slab surrounded by vacuum in a simulation box with periodic boundary conditions in the three spatial directions. The dimensions of the simulation cell were  $Lx = Ly = 54 \text{ \AA}$  with  $Lz = 3Lx$ , with  $z$  being the normal direction to the liquid-vapor interface. The GROMACS 4.5.4 package<sup>17,18</sup> was employed in all simulations presented in this work. The equations of motion were solved using the leapfrog algorithm with a time step of 1 *fs*. The temperature was coupled to the Nosé-Hoover thermostat with a parameter  $\tau_T = 0.2 \text{ ps}$  while the pressure was coupled to the Parrinello-Rahman barostat<sup>19</sup> with a coupling parameter  $\tau_P = 0.5 \text{ ps}$ .

We computed the electrostatic interactions with the particle mesh Ewald approach<sup>20</sup> with a tolerance of  $10^6$  for the real space contribution, with a grid spacing of 1.2 Å and spline interpolation of order 4. In the isotropic NPT simulations the real part of the Ewald summation and the LJ interactions were truncated at 9 Å. Long range corrections for the LJ energy and pressure were included. The dielectric constant is obtained from the analysis of the dipole moment fluctuations of the simulation system.<sup>21,22</sup> The density and the dielectric constant were calculated from the same simulation for at least 200 *ns* after an equilibration period of 10 *ns*. For the surface tension computations in the NVT ensemble the cutoff was

set to 26 Å, since the surface tension depends on the truncation of the interactions<sup>23</sup> and the interface cross-sectional area.<sup>24,25</sup> The equilibration period for the interfacial simulations was 2 *ns*, and the results for the average properties were obtained over an additional 10 *ns* trajectory.

The Berendsen barostat was employed For the calculation of the melting temperature and of the density of the ice. The use of this barostat allows the simulation box to expand or contract, and then to form ice or liquid phases. For studying the ice phase and the melting properties, the temperature was fixed with a Berendsen thermostat with a relaxation time of 0.2 *ps*.<sup>26</sup> For the description of the coexistence between liquid and solid water, we employed an orthogonal cell. This approach is consistent with the crystallographic data of the solid phase Ih.<sup>27</sup> The cell size is  $Lx = 21.6\text{Å}$ ,  $Ly = 23.3\text{Å}$  and  $Lz = 53.8\text{Å}$ . Which gives us a contact area between the  $Lx * Ly = 503.28\text{Å}^2$  phases.

## Results

First, we analyzed the water structure obtained using our model.. Differently from the rigid models, the FBA/ $\epsilon$  exhibits a distribution of HOH angles illustrated for 1 *bar* and 298 *K* in the figure 2(a). The average angle,  $108.56^\circ$  is close to the average experimental value<sup>2</sup> which is  $106^\circ$  and to the value employed for the rigid SPC model which is  $109.47^\circ$ . The distribution of O-H bond distances for the FBA/ $\epsilon$  model at 298 *K* and 1 *bar* is illustrated in the figure 2(b). This result shows the average bond distance at of 0.09495 *nm* what is 4% lower than the neutron diffraction value, 0.099 *nm*,<sup>28</sup> and only 2.4% lower than the X-ray diffraction value, 0.09724 *nm*.<sup>29,30</sup> In principle rigid models can be constructed to give this bond distance, however they can not accommodate the change with the temperature of the O-H bond distance observed both in the experiments and in our model. Figure 2(c) shows the distribution of dipole moments of the water molecules at 298 *K* and 1 *bar*. The mean dipole moment of the distribution is 2.42 *D*. Then, we test how robust is the parametriza-

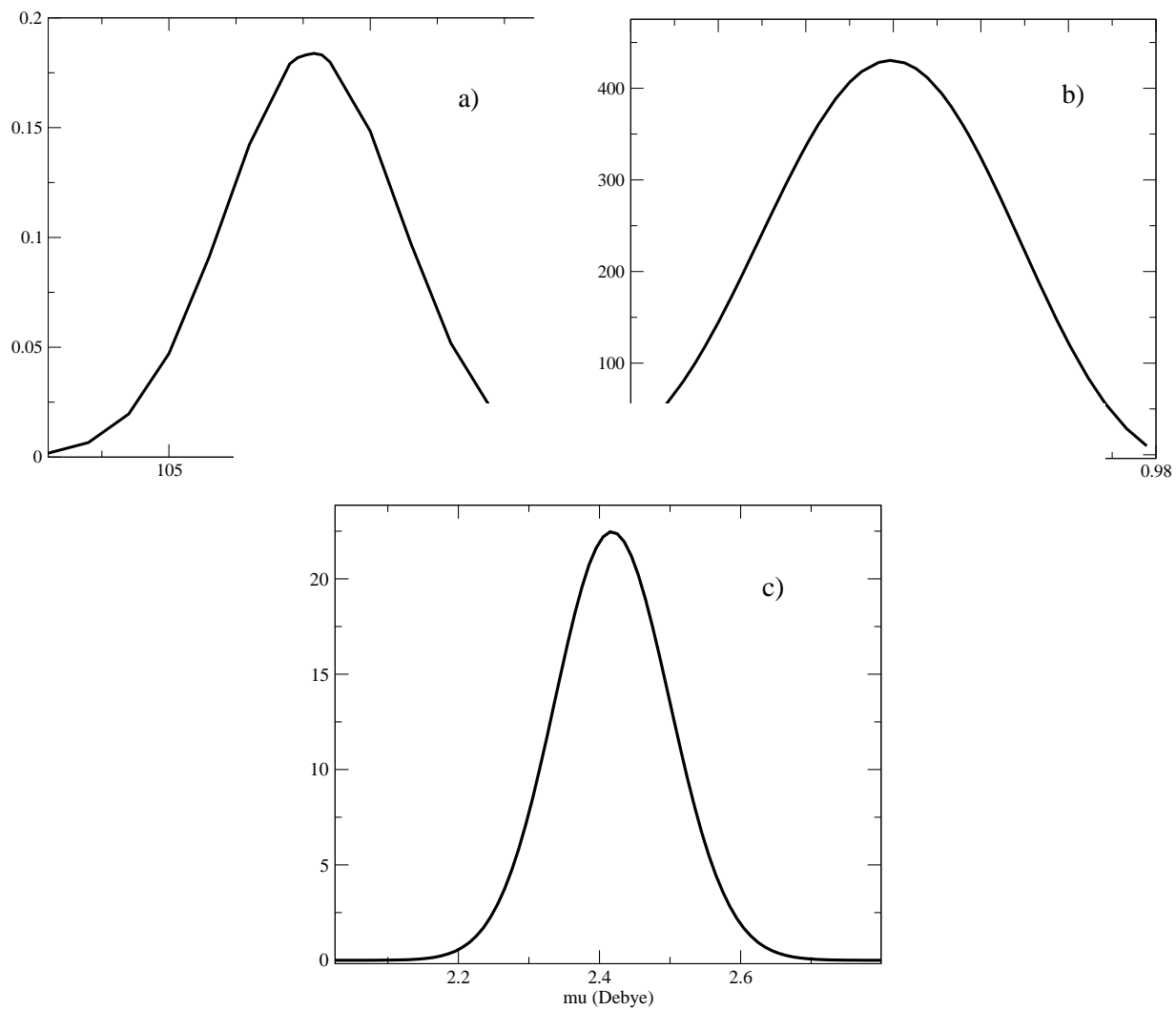


Figure 2: (a) HOH angle (b)O-H bond distance (c) dipole moment distributions at 298K and 1bar for the FBA/ $\epsilon$  model.



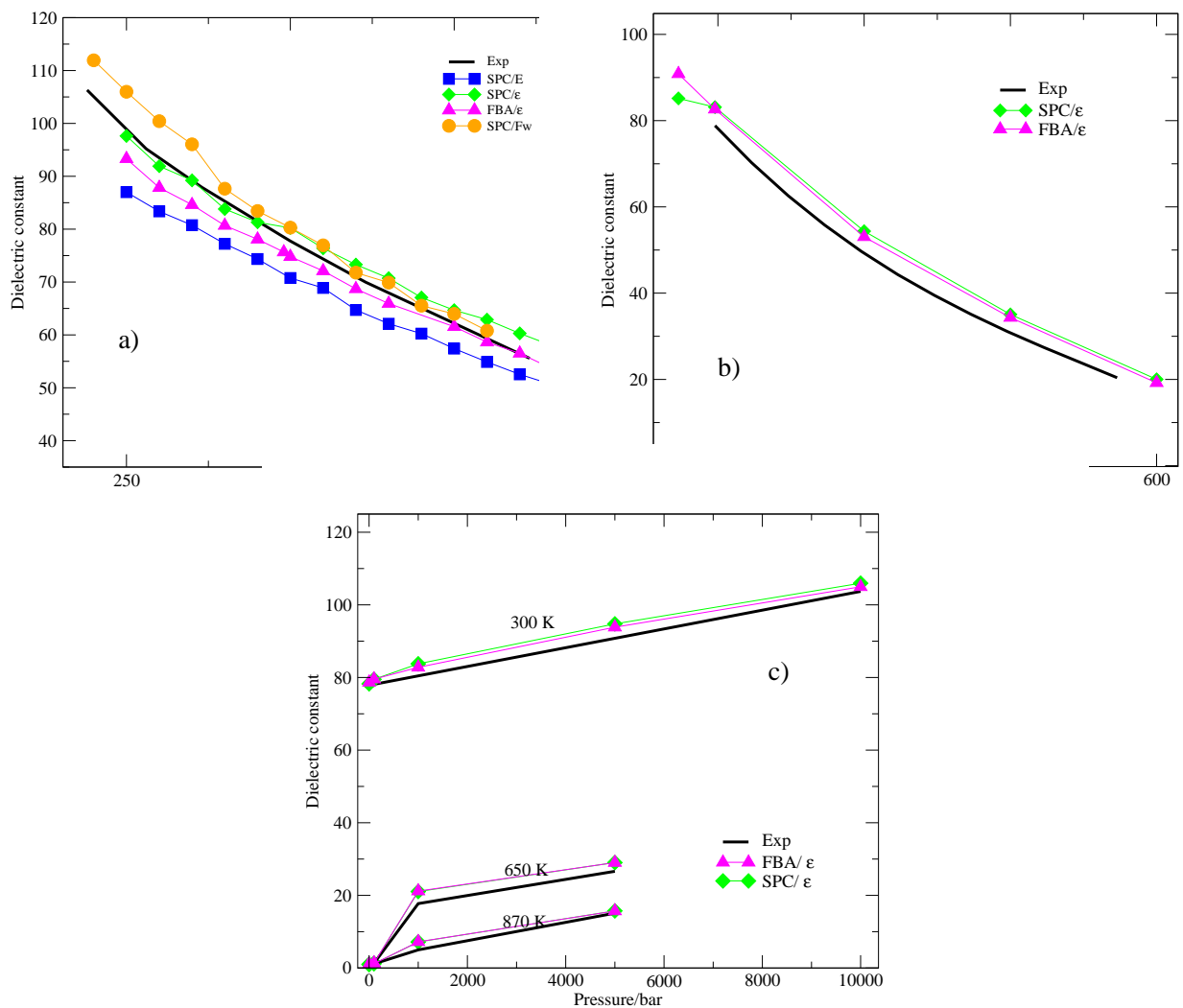


Figure 3: Dielectric constant (a) versus temperature at 1 bar, (b) at the liquid-vapor coexistence line and (c) versus pressure for three different temperatures SPC/ $E^{14}$ (squares), SPC/ $\epsilon^{14}$ (diamonds), FBA/ $\epsilon$  (triangles), SCP/Fw calculated here (circles) models and experimental data<sup>31</sup> (solid line).

tion regarding variations of temperature. The flexible FBA/ $\epsilon$  and the SPC/ $\epsilon$  models are parametrized to reproduce the experimental value of the dielectric constant,  $\epsilon$ , at 298 K and 1 bar with a 3.6 % of tolerance.<sup>32</sup> Figure 3 illustrates the dielectric constant,  $\epsilon$ , versus pressure for different temperatures at 1 bar and at the liquid-vapor coexistence for both models. The comparison between the FBA/ $\epsilon$ , the rigid model and the experiments indicates that flexibility does not adds better concordance with the data even if large changes in pressure and in temperature are implemented as shown in the figure 3(c).

The FBA/ $\epsilon$  model was also parametrized to reproduce the experimental density at 298 K and 1 bar.<sup>31</sup> The figure 4 shows the density as a function of the temperature for the FBA/ $\epsilon$ , SPC/E,<sup>14</sup> SPC/ $\epsilon$ ,<sup>14</sup> SPC/ $Fw$ <sup>5</sup> models and the experiments.<sup>31</sup> The non-polarizable models and the FBA/ $\epsilon$  agree with the experiments at 300K since they were parametrized to give the correct density at this temperature. The SPC/E,<sup>14</sup> however, at low temperatures overestimates the density, while both the SPC/ $\epsilon$ <sup>14</sup> and FBA/ $\epsilon$  agree with the experiments for a wide range of temperatures. The FBA/ $\epsilon$  at very low temperatures shows a small improvement over the SPC/ $\epsilon$ <sup>14</sup> model. A consequence of a good parametrization of the density for a wide range of temperatures can be observed in the behavior of the response functions. Response functions exhibit a very peculiar behavior in water. The thermal expansion coefficient,  $\alpha$ , which for most materials is almost constant or slightly increases with the temperature, for water it decreases abruptly with the decrease of the temperature and it becomes negative. The compressibility for a number of materials increases monotonically with the temperature but in the case of water it has a minimum. Figure 5 illustrates both  $\alpha$  and  $\kappa_T$  as a function of temperature for SPC/E, SPC/ $\epsilon$ , FBA/ $\epsilon$  models and the experimental results.<sup>31</sup> At low temperatures the FBA/ $\epsilon$  model gives the better approximation to the experimental data.<sup>31</sup> In the particular case of the compressibility, the flexible model shows the minimum approximately in the same temperature as the experiments while the non-polarizable force fields present a shift. Next we check if the flexible model also presents a good agreement with the experiments for high temperatures at the vapor phase given the parametrization

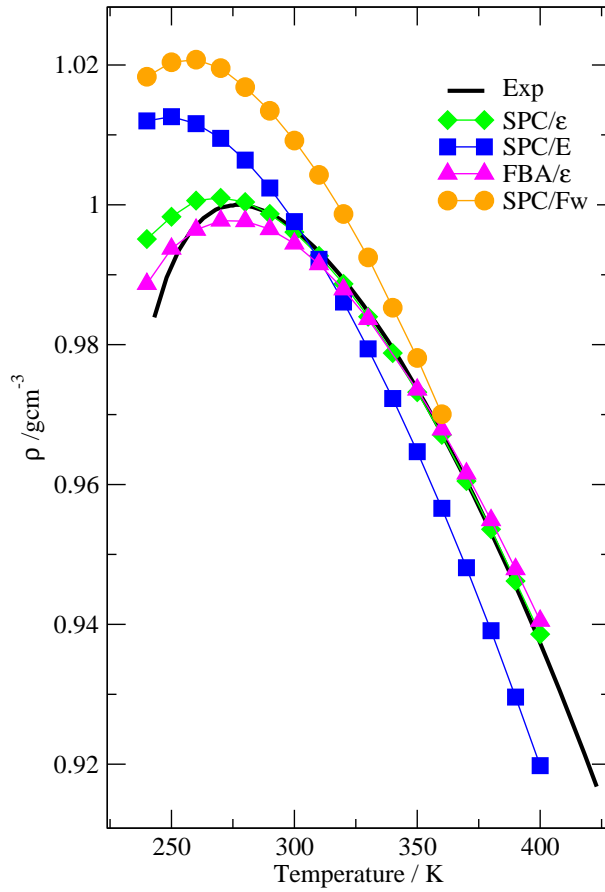


Figure 4: Density as a function of temperature at 1 bar for the SPC/E<sup>14</sup>(squares), SPC/ε<sup>14</sup>(diamonds), FBA/ε (triangles), SCP/Fw calculated here (circles) models and experimental data<sup>31</sup> (solid line).

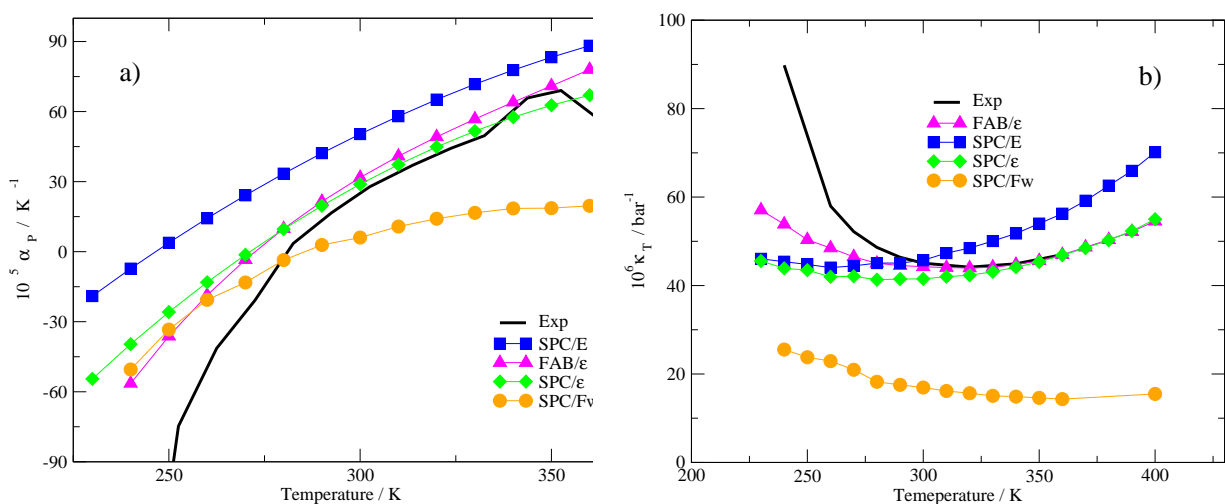


Figure 5: (a) Thermal expansion coefficient and (b) isothermal compressibility as a function of temperature at pressure constant of 1bar for the SPC/E<sup>14</sup>(squares), SPC/ $\epsilon$ <sup>14</sup>(diamonds), FBA/ $\epsilon$  (triangles), SCP/Fw calculated here (circles) models and experimental data<sup>31</sup> (solid line).

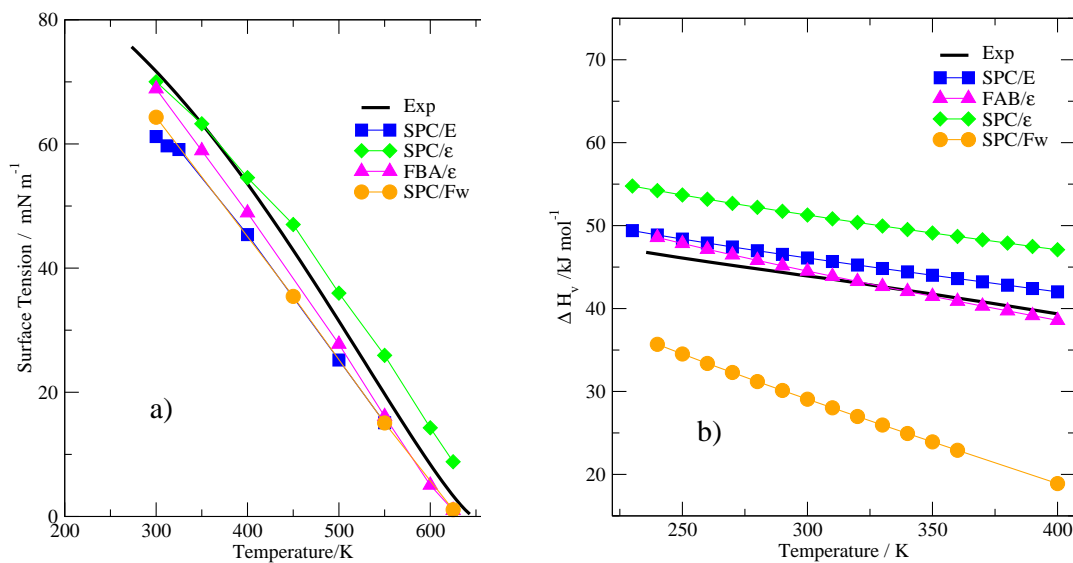


Figure 6: (a) Surface tension and (b) heat of vaporization as a function of temperature at pressure constant of 1bar for the SPC/E<sup>14</sup>(squares), SPC/ $\epsilon$ <sup>14</sup>(diamonds), FBA/ $\epsilon$  (triangles), SCP/Fw calculated here (circles) models and experimental data<sup>31</sup> (solid line).

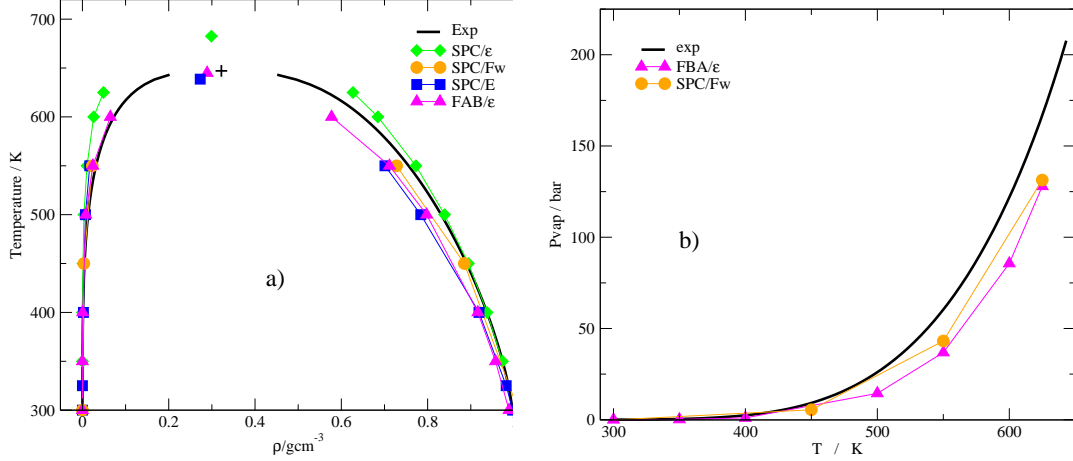


Figure 7: Temperature versus density phase diagram for the SPC/E<sup>14</sup>(squares), SPC/ $\epsilon$ <sup>14</sup>(diamonds), FBA/ $\epsilon$  (triangles), SCP/Fw calculated here (circles) models and experimental data<sup>31</sup> (solid line).

was performed at the low temperatures and densities. One important property in which the flexibility might matter is the surface tension. For testing the behavior at high temperatures we selected the surface tension. The surface tension versus temperature is shown in the figure 6(a). The flexible model shows a consistent agreement with the experiment while the rigid models fit the data either at low or high temperatures but not for both ranges. As the temperature is increased, it is not clear how the HOH angle and the OH bond might change. In order to check this we look at the liquid-vapor transition. Figure 6(b) compares the heat of vaporization as a function of the temperature at 1 *bar* for the SPC/E<sup>14</sup>(squares), SPC/ $\epsilon$ <sup>14</sup>(solid diamonds), FBA/ $\epsilon$  (triangles) models with the experimental data<sup>31</sup> (solid line). It shows that both rigid SPC/ $\epsilon$  and flexible FBA/ $\epsilon$  agree with the data what suggests that the flexibility is not so relevant for the vapor heat specifically but might affect coexistence properties. In order to check this point, we also obtain the gas-liquid phase diagram. The coexisting densities were estimated from the average density profile in the liquid and vapor regions of the slab. Figure 7(a) shows the temperature versus density phase diagram for the SPC/E<sup>14</sup>(squares), SPC/ $\epsilon$ <sup>14</sup>(diamonds), FBA/ $\epsilon$  (triangles) models and experimental data<sup>31</sup> (solid line). The flexible model improves the agreement with experiment significantly compared to the rigid models for the gas phase and for the critical temperature and density.

The vapor pressure is calculated as the normal component of the pressure tensor in the interface simulations. Consistent with the improved results for the gas phase, figure 7(b) shows that the new force field reproduces the curvature of vapor pressure when compared with the experiments.<sup>31</sup>

Finally, a comprehensive comparison between the results obtained by our flexible model compared with its non-polarizable approaches is presented in the Table 2. Following the notation introduced by Vega et al.,<sup>9</sup> the models are evaluate by a score. The final score of the FBA/ $\epsilon$  is higher than the non-polarizable models.

## Conclusions

We introduced a new 3 sites flexible model, the FBA/ $\epsilon$  which was parametrized using the experimental values of the density, the dielectric constant and the dipole moment at 1 *bar* and 240 *K*.

This approach gives a bond and angle distribution comparable with experimental results. It is also able to produce good agreement with the experiments for thermodynamic and structural properties at low and high temperatures. In particular the flexibility allow for the model to provide a good coexistence region of the density versus temperature phase diagram. The major advantage of the model is that is able to reproduce with accuracy a wide range of properties what at different temperature. This robust behavior makes it a good candidate for studying mixtures of water and other polar materials.

**Table 2: Experimental and simulation data results of 3 sites water models. The thermodynamic conditions are reported according to the calculated property.**

Property	Experimental data	SPC/E	SPC/ $\epsilon$	FBA/ $\epsilon$	Tolerance (%)	SPC/E score	SPC/ $\epsilon$ score	FBA/ $\epsilon$ score
Enthalpy of phase change / kcal mol <sup>-1</sup>								
$\Delta H_{melt}$	1.44	0.74	5.38	2.14	5	0.3	0.0	0.3
$\Delta H_{vap}$	10.52	11.79	12.25	10.69	2.5	5.2	3.4	9.4
Critical point properties								
$T_c/K$	647.1	638.6	682.6	642	2.5	9.5	7.8	9.7
$\rho_c/g\text{ cm}^{-3}$	0.322	0.273	0.299	0.299	2.5	3.9	7.1	7.1
$p_c/\text{bar}$	220.64	139	167	167	5	2.6	5.1	5.1
Surface tension/mN m <sup>-1</sup>								
$\gamma_{300K}$	71.73	63.6	70.02	73.98	2.5	5.5	9.0	8.7
$\gamma_{450K}$	42.88	36.7	47	46.2	2.5	4.2	6.2	6.9
Melting properties								
$T_m/K$	273.15	215	200	243	2.5	1.5	0.0	5.6
$\rho_{liq}/g\text{ cm}^{-3}$	0.999	1.011	0.9864	0.9901	0.5	7.6	7.5	8.2
$\rho_{sol}/g\text{ cm}^{-3}$	0.917	0.95	0.8932	0.945	0.5	2.8	4.8	3.9
$dp/dT\text{ (bar K}^{-1}\text{)}$	-137	-126.05	-591.52	-424.982	5	8.4	0.0	0.0
Orthobaric densities and temperature of maximum density <b>TMD</b>								
<b>TMD/K</b>	277	241	266	275.4	2.5	4.8	8.4	9.8
$\rho_{298K}/g\text{ cm}^{-3}$	0.997	0.994	0.9964	0.9948	0.5	9.4	9.9	9.6
$\rho_{400K}/g\text{ cm}^{-3}$	0.9375	0.916	0.9385	0.9406	0.5	5.4	9.8	9.3
$\rho_{450K}/g\text{ cm}^{-3}$	0.8903	0.86	0.8893	0.8982	0.5	3.2	9.8	8.2
Isothermal compressibility / 10 <sup>-6</sup> bar <sup>-1</sup> )								
$\kappa_T\text{ [1 bar; 298 K]}$	45.3	46.1	41.4	45.6	5	9.6	8.3	9.9
$\kappa_T\text{ [1 bar; 360 K]}$	47	57.7	46.86	47.2	5	5.4	9.9	9.9
Thermal expansion coefficient / 10 <sup>3</sup> K <sup>-1</sup> )								
$\alpha_P\text{ [1 bar; 298 K]}$	22.66	48.6	26.9	29.5	5	0.0	6.3	4.0
$\alpha_P\text{ [1 bar; 350 K]}$	68.2	83.23	62.56	71	5	5.6	8.3	9.2
Gas properties								
$\rho_v\text{ [350 K] (bar)}$	0.417	0.14	0.042	0.224	5	0.0	0.0	0.7
$\rho_v\text{ [450 K] (bar)}$	9.32	5.8	1.88	5	5	2.4	0.0	0.7
Heat capacity at constant pressure/cal mol <sup>-1</sup> K <sup>-1</sup>								
$C_p\text{ [liq 298 K; 1 bar]}$	18	20.7	20.6	20.7	5	7.0	7.1	7.0
$C_p\text{ [ice 250 K; 1 bar]}$	8.3	14.9	14.8	14.9	5	0.0	0.0	0.0
Static dielectric constant								
$\epsilon\text{ [liq; 298 K]}$	78.5	68	78.3	75.5	2.5	4.6	9.9	8.5
$\epsilon\text{ [liq; 350 K]}$	62.12	57.45	64.65	61.49	2.5	7.0	8.4	9.6
$\epsilon\text{ [10kbar, 300K]}$	103.63	91.3	106.65	104.9	2.5	5.2	8.8	9.5
$\epsilon\text{ [I}_h\text{; 240 K]}$	107	39	23	39.5279	2.5	0.0	0.0	0.0
$T_m$ -TMD- $T_c$ ratios								
$T_m\text{ [I}_h\text{]}/T_c$	0.422	0.337	0.286	0.378	5	6.0	3.6	7.9
TMD/ $T_c$	0.428	0.378	0.381	0.428	5	7.7	7.8	10.0
TMD- $T_m\text{ (K)}$	4	26	66	32.4	5	0.0	0.0	0.0
Densities of ice polymorphs/g cm <sup>-3</sup>								
$\rho\text{ [I}_h\text{ 250 K; 1 bar]}$	0.92	0.944	0.907	0.94	0.5	4.8	7.2	5.7
$\rho\text{ [II 123 K; 1 bar]}$	1.19	1.245	1.18	1.245	0.5	0.8	8.3	0.8
$\rho\text{ [V 223 K; 5.3 kbar]}$	1.283	1.294	1.273	1.294	0.5	8.3	8.4	8.3
$\rho\text{ [VI 225 K; 11 kbar]}$	1.373	1.403	1.33	1.403	0.5	5.6	3.7	5.6
EOS high pressure								
$\rho\text{ [373 K; 10 kbar]}$	1.201	1.213	1.2034	1.215	0.5	8.0	9.6	7.7
$\rho\text{ [373 K; 20 kbar]}$	1.322	1.338	1.3219	1.339	0.5	7.6	10.0	7.4
Self-diffusion coefficient/cm <sup>2</sup> s <sup>-1</sup>								
$\ln D_{278K}$	-11.24	-11.08	-11.69	-11.58	0.5	7.2	2.0	4.0
$\ln D_{298K}$	-10.68	-10.58	-11.08	-11.01	0.5	8.1	2.5	3.8
$\ln D_{318K}$	-10.24	-10.24	-10.72	-10.71	0.5	10.0	0.6	0.8
$E_a\text{ k}_J\text{ mol}^{-1}$	18.4	15.4	17.82	15.98	5	6.7	9.4	7.4
Shear viscosity / mPa s								
$\eta\text{ [1 bar; 298 K]}$	0.896	0.729	1.259	0.9443	5	6.3	1.9	8.9
$\eta\text{ [1 bar; 373 K]}$	0.284	0.269	0.378	0.3259	5	8.9	3.4	7.0
Orientational relaxation time / ps								
$\tau_2^{OH}\text{ [1 bar; 298 K]}$	2.36	1.9	1.97	2.1	5	6.1	6.7	7.8
Structure								
$\chi^2\text{ (F(Q))}$	0	17.7	17.2	18.1	5	8.0	8.0	8.0
$\chi^2\text{ (overall)}$	0	22.2	21.9	22.6	5	7.0	7.0	7.0
Phase diagram								
Overall score (out of 10)						5.4	5.7	6.5

## **Acknowledgements**

We thank the Brazilian agencies CNPq, INCT-FCx, and Capes for the financial support.  
We also thank the SECITI of Mexico city for financial support.



## References

- (1) Hasted, J. B. Liquid water: Dielectric properties, in *Water A comprehensive treatise*, Vol 1, Ed. F. Franks Plenum Press, New York, 1972, pp. 255-309.
- (2) Ichikawa, K. Kameda, Y. Yamaguchi, T. Wakita, H. Misawa, M. Neutron-diffraction investigation of the intramolecular structure of a water molecule in the liquid phase at high temperatures *Mol. Phys.* **1991**, 73, 79.
- (3) Furlan, A; Lomba, E.; Barbosa, M. C. Temperature of maximum density and excess properties of short-chain alcohol aqueous solutions: A simplified model simulation study. *J. Chem. Phys.* **2017** 146, 144503.
- (4) Kim, J. S.; Morrow, A. R.; Yethira, A.; Yethiraj, A. Self-Diffusion and Viscosity in Electrolyte Solutions. *J. Phys. Chem. B* **2012**, 116, 12007-12013.
- (5) Wu, Y. J.; Tepper, H. L.; Voth, G. A. Flexible simple point-charge water model with improved liquid-state properties. *J. Chem. Phys.* **2006**, 124, 024503.
- (6) González, M. A.; Abascal, J. L. F. A flexible model for water based on TIP4P/2005. *J. Chem. Phys.* **2011**, 135, 224516-.
- (7) Barrat, L.; McDonald, I. R. The role of molecular flexibility in simulations of water. *Mol. Phys.* **1990**, 70, 535-539.
- (8) Smith, D. E.; Haymet, A. D. J. Structure and dynamics of water and aqueous solutions: The role of flexibility. *J. Chem. Phys.* **1992**, 96, 8450-8459.
- (9) Vega, C.; Abascal J. L. F. Simulating water with rigid non-polarizable models: a general perspective. *Phys. Chem. Chem. Phys.* **2011**, 13, 19663-19688.
- (10) Warshel, A. *Computer Modeling of Chemical Reactions in Enzymes and Solutions*. Wiley, New York, 1991.

- (11) Schmitt, U. W.; Voth, G. A. Multistate Empirical Valence Bond Model for Proton Transport in Water. *J. Phys. Chem. B.* **1998**, 102, 5547-5551.
- (12) Schmitt, U. W.; Voth, G. A. The computer simulation of proton transport in water. *J. Chem. Phys.* **1999**, 111, 9361-9381.
- (13) López-Lemus, J.; Chapela, G.A.; Alejandre, J. Effect of flexibility on surface tension and coexisting densities of water. *J. Chem. Phys.* **2008**, 128, 174703.
- (14) Fuentes-Azcatl, R. Mendoza, N. Alejandre, J.; Improved SPC force field of water based on the dielectric constant: SPC/ $\epsilon$ . *J. Physica A.* **2015**, 420, 116-123.
- (15) Fuentes-Azcatl, R.; Barbosa, M. C. Thermodynamic and dynamic anomalous behavior in the TIP4P/ $\epsilon$  water model. *Physica A.* **2016**, 444, 86-94.
- (16) Fuentes-Azcatl R.; Alejandre, J.; Non-Polarizable Force Field of Water Based on the Dielectric Constant: TIP4P/ $\epsilon$ . *J. Phys. Chem. B.* **2014**, 118, 1263-1272.
- (17) Hess, B.; Kutzner, C.; van der Spoel, D.; Lindahl, E. GROMACS 4.5 Algorithms for Highly Efficient, Load-Balanced, and Scalable Molecular Simulation. *J. Chem. Theory Comput.* **2008**, 4, 435-447.
- (18) van der Spoel, D.; Lindahl, E.; Hess, B.; Groenhof, G.; Mark, A. E.; Berendsen, H. J. C. GROMACS: fast, flexible, and free. *J. Comput. Chem.* **2005**, 26, 1701-1718.
- (19) Parrinello, M.; Rahman, A. Polymorphic Transitions in Single Crystals: A New Molecular Dynamics Method. *J. Appl. Phys.* **1981**, 52, 7182-7190.
- (20) Essmann, U.; Perera, L.; Berkowitz, M. L.; Darden, T.; Lee, H.; Pedersen, L. G. A smooth particle mesh Ewald method. *J. Chem. Phys.* **1995**, 103, 8577-8592.
- (21) Hansen, J. P.; McDonald, I. R. Theory of Simple Liquids, 4th ed.; Elsevier: Amsterdam, 2013.

- (22) Neumann, M. Dipole moment fluctuation formulas in computer simulations of polar systems. *Mol. Phys.* **1983**, 50, 841-845.
- (23) Truckymchuk, A.; Alejandre, J. Computer simulations of liquid/vapor interface in Lennard-Jones fluids: Some questions and answers. *J. Chem. Phys.* **1999**, 111, 8510-8523.
- (24) Orea, P.; López-Lemus, J.; Alejandre, J. Oscillatory surface tension due to finite-size effects. *J. Chem. Phys.* **2005**, 123, 114702-114813.
- (25) Gonzalez-Melchor, M.; Bresme, F.; Alejandre, J. Molecular dynamics simulations of the surface tension of ionic liquids. *J. Chem. Phys.* **2005**, 122, 104710-104718.
- (26) Garcia Fernández R.; Abascal, J. L.; Vega, C. The melting point of ice Ih for common water models calculated from direct coexistence of the solid-liquid interface. *J. Chem. Phys.* **2006**, 124, 144506.
- (27) Petrenko, V. F.; Whitworth, R. W. *Physics of Ice*. Oxford University Press, Oxford, 1999.
- (28) Zeidler, A. Salmon, P.S.Fischer, H. E. Neufeind, J. C. Simonson J. M. Markland, T.E. Isotope effects in water as investigated by neutron diffraction and path integral molecular dynamics, *J. Phys.: Condens. Matter* **2012**, 24, 284126.
- (29) Narten, A. H. Levy, H. A. *Liquid Water: Molecular Correlation Functions from X Ray Diffraction*. *J. Chem. Phys.* **1971** , 55, 2263-2269.
- (30) Tomberli, B. Benmore, C. J. Egelstaff, P. A. Neufeind, J. Honkimaki, V. Isotopic quantum effects in water structure measured with high energy photon diffraction *J. Phys.:Condens. Matter*. **2000**, 12, 2597-2612.
- (31) Lemmon, E. W.; McLinden, M. O.; Friend, D. G. *Thermophysical Properties of Fluid*

Systems, NIST Chemistry WebBook, NIST Standard Reference Database; Linstrom, P.J., Mallard, W.G., Eds.; 2005; <http://webbook.nist.gov> (accessed July 1, 2016).

- (32) Pedro Fernandez Prini; International Association for the Properties of Water and Steam; <http://www.iapws.org/relguide/IF97-Rev.pdf>,2007 (accessed June 1, 2016).